Journal of Theoretical and Applied Information Technology
31st July 2024. Vol.102. No. 14

ISSN: 1992-8645 www.jatit.org E-ISSN: 1817-3195

MAYFLY OPTIMIZATION WITH DEEP LEARNING ASSISTED GLAUCOMA DIAGNOSIS ON RETINAL FUNDUS IMAGES

ANITA MADONA M [1], DR. PANNEER AROKIARAJ S [2]

[1]Research Scholar, Department of Computer Science, Thanthai Periyar Govt Arts and Science College (Autonomous), Affiliated to Bharathidasan University, Tiruchirappalli, India
[2]Assosiate Professor, Department of Computer Science, Thanthai Periyar Govt Arts and Science College (Autonomous), Affiliated to Bharathidasan University, Tiruchirappalli, India
E-mail: [1]madonaphd@gmail.com, [2]drpancs@gmail.com

ABSTRACT

Glaucoma is a chronic eye disease that causes vision impairment if not diagnosed and treated at earlier stages. Timely detection may save patients from permanent loss of vision. Physical examination of glaucoma by ophthalmologists contains costly, time-consuming, and skill-oriented processes. Various approaches are in investigational stage for identifying earlier-stage glaucoma, however, a sure diagnostic method remains challenging. Medical check-ups to observe the retinal area are occasionally required by ophthalmologists, who need a considerable number of experience and skill to appropriately interpret the outcomes. To overcome these issues, algorithm based on deep learning (DL) technique has been developed to examine imageries of optic nerve and retinal structures and to diagnose and screen glaucoma based on retinal input images. This article introduces a new Mayfly Optimization with Deep Learning Assisted Glaucoma Detection and Classification (MFODL-GDC) technique on Retinal Fundus Images. The MFODL-GDC technique aims to segment and categorize the retinal images for classification of Glaucoma. In the presented MFODL-GDC technique, bilateral filtering and CLAHE-based contrast enhancement are involved in image preprocessing. Besides, the MFODL-GDC technique applies Quick CapsNet model for optic disc (OD) and optic cup (OC) segmentation. Moreover, the MFODL-GDC technique uses DenseNet121 model for feature extraction and its hyperparameter tuning process can be performed by the use of the MFO algorithm. Furthermore, extreme learning machine (ELM) model can be exploited for the detection and classification process. The extensive performance validation of the MFODL-GDC technique is tested on benchmark datasets. The widespread comparison research stated that supremacy of MFODL-GDC technique over current techniques.

Keywords: *Glaucoma Screening; Computer-Aided Diagnosis; Retinal Fundus Imaging; Deep Learning; Mayfly Optimization*

1. INTRODUCTION

Glaucoma is an eye illness that can be related to the damage of retinal ganglion cells where their axons progressively worsen after a period of time that results in long-lasting vision loss once the disorder goes untreated [1]. The possibility of acquiring glaucoma can be further raised by other factors like family history, race, and age. Wide-ranging eye analysis employing assessment of the optic nerve head, sight field tests, and tonometry can be essential measures for identifying glaucoma [2]. However, these tests commonly consume long period, expensive, and need specialized equipment and specialists. Because of these limitations, there is a growing tendency to implement deep learning (DL) techniques for automatically identifying glaucoma utilizing fundus images [3]. Fundus imaging has non-invasive modality, which can be simply available and offers crucial data regarding eye and optic nerve heads, containing structural modifications employed in order to specify glaucoma existence [4]. These images are obtained as comprehensive information of all

features of the retina, comprising the color, shape, and size of important areas namely the fovea optic disc (OD), blood vessels, optic cup (OC), and neuroretinal rim [5].

Recently, Artificial intelligence (AI) technologies have been considerably developed. Several researches have been carried out in medical field to combine AI methodology for real-world medical treatments [6]. Computer-aided diagnosis (CAD) systems for identifying glaucoma, can be normal in medical applications [7]. The applications of ML and more recent deep learning (DL) methods have improved the diagnostic outcome of these automatic equipment for diagnosing glaucoma. Despite the impossibility of population screening for glaucoma by standard system [8], DL particularly convolutional neural networks (CNNs) are extensively employed in the domain of medical images as well as deliberated pattern identification tools, which support for identification of eye diseases, recommending for instances, various approaches and techniques to diagnose diseases like glaucoma and cataracts from digital images [9]. The application of DL is exhibited in analysis of diabetic retinopathy (DR) detection on a large scale. This development is due to numerous aspects namely the expansion of complex methods and the accessibility of fundus image databases for this research [10].

This manuscript concentrates on development of Mayfly Optimization with Deep Learning Assisted Glaucoma Detection and Classification (MFODL-GDC) technique on Retinal Fundus Images. The MFODL-GDC technique follows bilateral filtering and CLAHE-based contrast enhancement for image preprocessing. Also, the MFODL-GDC technique applies Quick CapsNet (QCN) model for optic disc (OD) and optic cup (OC) segmentation. Meanwhile, the MFODL-GDC technique uses DenseNet121 model for feature extraction and its hyperparameter tuning process can be performed by the use of the MFO algorithm. Furthermore, extreme learning machine (ELM) model can be exploited for the detection and classification process. The extensive performance validation of the MFODL-GDC technique is tested on benchmark datasets.

2. RELATED WORKS

Lenka et al. [11] introduced study to develop and train various multi-task DL methods for automatic retinal image classification and segmentation. The multi-task architecture was learned for segmentation process of OD and OC as well as classification process for accurately identifying glaucoma employing both image and structural-based features. This multi-tasking architecture developed an adapted U-net model in that Mobile-Netv2 could be employed in encoder function, Graph Convolution Network (GCN) has been exploited in decoder function, and attention module (AM) was utilized for determining the RoI for improved feature extraction. Kamara et al. [12] developed a technique with 2 stages, first stage was the method without feature selection (FS) and in second stage, the authors implemented FS approaches and compared outcomes. This can be dependent upon superpixel method and supervised ML after a second phase, the authors execute FS to choose the highly important features for enhancing the effectiveness, decreasing data dimensionality and minimizing elapsed time, lastly, the authors implemented the support vector machine (SVM) method.

Shyamalee and Meedeniya [13] presented a computational technique for dividing and categorizing retinal fundus imageries for diagnosing glaucoma. Various data augmentation algorithms are implemented to avoid overfitting whereas utilizing numerous data preprocessing techniques to increase the image quality and attain higher accurateness. The subdivision methods depend on the attention U-Net with 3 different CNN models namely ResNet50, Inceptionv3, and VGG19. Phasuk et al. [14] projected an automatic glaucoma screening technique employing retinal fundus images through ensemble model for combining the outcomes of diverse detection models and these are provided as the inputs to a modest

artificial neural networks (ANNs) for acquiring the end outcomes.

In [15], a robust DL-based CNNs model was designed to manage the issue. The network contains 6 convolutional layers with variety of activation functions, and pooling layers to obtain the theoretical and comprehensive data of the input images. Manikandan et al. [16] intended to design a CAD technique for diagnosing glaucoma in fundus images. In this study, the authors introduced an approach for automated outline of the OD in a retinal image by automatic thresholding method. The OC was divided based on marker-controlled automatic watershed conversion. The OC to disc ratio (OCDR) can be evaluated to demonstrate the existence of glaucoma.

3. THE PROPOSED MODEL

In this study, we have devised and proposed an automated glaucoma classification process, called technique on Retinal Fundus Images. The MFODL-GDC technique aims to divide and categorize the retinal images for Glaucoma identification. It comprises several stages of operations namely image preprocessing, QCN segmentation, DenseNet feature extraction, MFO-based hyperparameter tuning, and ELM classification. Figure 1 shows the entire flow of MFODL-GDC algorithm.

3.1. Image Pre-processing

The combination of Contrast Limited Adaptive Histogram Equalization (CLAHE) and bilateral filtering (BF) is a powerful tool for improving image quality and diagnostic accuracy in the preprocessing of fundus images, [17]. BL helps smooth the image and reduce noise while maintaining structures and important edges, making it very efficient for retaining crucial data in medical images like fundus scans. Meanwhile, CLAHE is used to address the issue by adaptively redistributing pixel intensity, thereby enhancing the visibility of subtle anomalies and features. Both approaches provide a complete preprocessing method which improves fundus images, ensuring that medical experts can make accurate assessments of visual health and identify conditions such as macular degeneration or diabetic retinopathy.

3.2. Image Segmentation

For the segmentation of OC and OD, the QCN model is utilized. QCN is used for performing the segmentation process, an extension of Capsule Network [18]. In this section, the structure of QCN is elaborated. In classical Capsule Network, two Conv layers that extract the input basic features of images are the first layers of the network. 8D vectors are generated by restructuring the second output of Conv layer. The term “Principal Capsule” represents 8D vectors. There might be multiple layers when the preliminary layer of capsule is generated. In the Conv layer of Quick-CapsNet, the kernel size of 9 denotes the size of window or filter that moves over the input image for performing convolution. Particularly, 9x9 kernels are used for extracting features from the input image that is utilized as input to succeeding layers in the network. The selection of kernel size may affect the network performance since it defines the quantity of spatial information taken from the input images. A small kernel size captures more local features, whereas large size captures more global features.

3.3. Optimal DL-based Feature Extraction

The DenseNet121 model is used to derive features from the segmented fundus images. DenseNet-121 is a DCNN structure known for its strong performance and efficiency in different computer vision tasks, namely object detection and image classification [19]. It stands out from classical CNN by introducing a dense connectivity pattern, where each layer is interconnected to the previous layer and all subsequent layers. This dense connectivity facilitates feature reuse and encourages the gradient flow, which alleviates the gradient vanishing problems. Compared to many other architectures, DenseNet-121 includes four densely connected blocks, involving transition and convolutional layers, which makes it a parameter-effective model that accomplishes

Journal of Theoretical and Applied Information Technology
31st July 2024. Vol.102. No. 14

ISSN: 1992-8645 www.jatit.org E-ISSN: 1817-3195

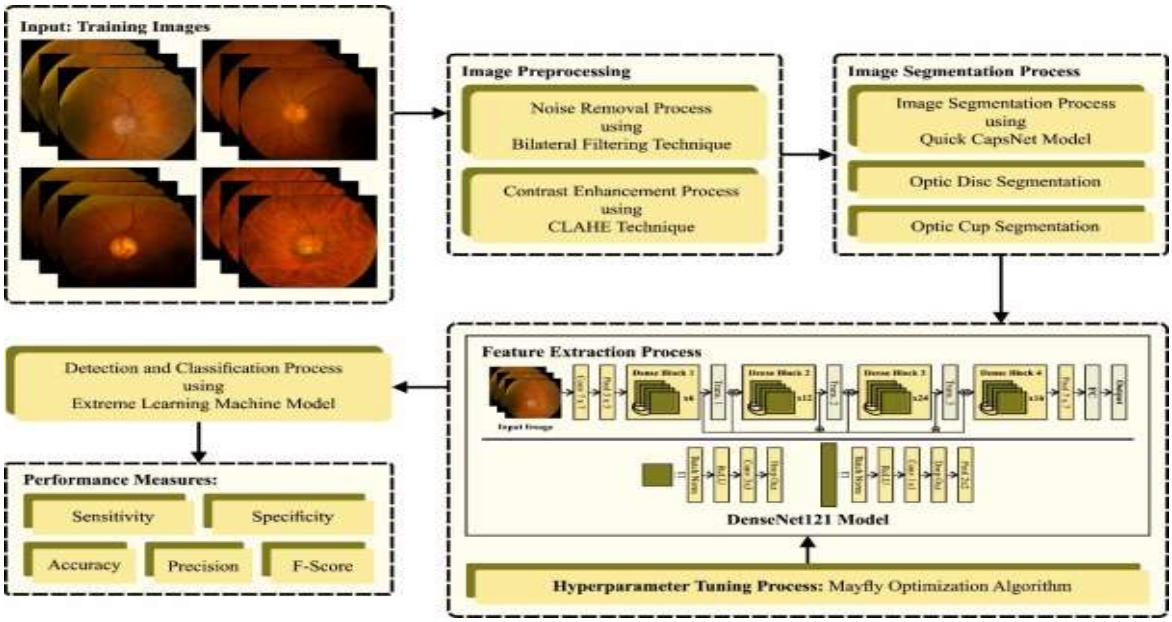

Figure 1: Overall flow of MFODL-GDC algorithm

extraordinary performance with fewer parameters. Its capability to extract highly discriminatory features from images has made it an invaluable tool to improve the performance of medical diagnoses and enable the development of advanced clinical decision support systems. In addition, its architecture encourages feature reuse, which is particularly beneficial while enhancing the robustness of diagnostic models and handling limited medical imaging data.

The MFO algorithm can be used to improve the performance of DenseNet121 architecture. MFO algorithm is inspired by the social behaviors of mayfly (MF), particularly the mating procedure, which achieve a better balance between global development and local exploration and can converge rapidly [20]. In the MPPT-based MA algorithm, the location of every individual MF signifies the reference voltage in MPPT control, and the changing tendency of reference voltage represents speed. Through the algorithm mechanism, the MA aims at changing the reference voltage of PV array and comparing the output power of PV array before and after the changes to find the optimum reference voltage values. The population has male and female individual MFs. The male MF gathers in-group, and according to the adjacent individuals and its own experience, the location of every male individual is updated. The location of i^{th} male MFs in the search space at t time is $m_{i,t}$, and the location is updated by adding $v_{i,t+1}$ velocity to the existing location:

$$m_{i,t+1} = m_{i,t} + v_{i,t+1} \quad (1)$$

$$v_{i,t+1} = g v_{i,t} + \alpha_1 e^{-\beta r_p^2}\left(p_{best,i} - m_{i,t}\right) + \alpha_2 e^{-\beta r_g^2}\left(g_{best} - m_{i,t}\right) \quad (2)$$

Here the speed of i^{th} male MF at t time is $v_{i,t}$. The gravity coefficient is g. The positive attraction constant exploited for scaling the input of cognitive and social components are α_1 and α_2, correspondingly. The past optimum reference voltage of i^{th} male MF is $p_{best,i}$. The Cartesian distance between m_i and g_{best} is r_g. The global optimum reference voltage amongst male MFs is g_{best}. The fixed visibility coefficient is β. The Cartesian distance between m_i and $p_{best,i}$ is r_p. The optimum individuals in the group continue to implement its up-and-down moving. Therefore, the optimal male MF continuously changes its velocity as follows:

$$v_{i,t+1} = v_{i,t} + dr \quad (3)$$

In Eq. (3), the nuptial dance coefficient is d and a randomly generated integer within $[-1, 1]$ is r.

Female MFs move towards male MFs to reproduce. The location of i^{th} female MF at t time is $f_{i,t}$, then the $positionf_{i,t+1}$ of the i^{th} female MF at $t+1$ time is

$$f_{i,t+1} = f_{i,t} + v_{i,t+1} \quad (4)$$

The speed of female MF relies on the behaviors of male MF. Consider that the study aims to increase the output power, and then the velocity $v_{i,t+1}$ of i^{th} female MF is updated as follows:

$$v_{i,t+1} = \begin{cases} gv_{i,t} + \alpha_2 e^{-\beta r_{mf}^2}(m_{i,t} - f_{i,t}) & P(f_{i,t}) < P(m_{i,t}) \\ gv_{i,t} + \lambda r & P(f_{i,t}) \geq P(m_{i,t}) \end{cases} \quad (5)$$

In Eq. (5), the random walking coefficient is λ. The Cartesian distance between m_i and f_i is r_{mf}. The output power of MF is P. The male individuals will move at random fashion when the female is not attracted to the male.

The mating process between both MFs is given in the following: one parent is nominated from the male population, and another from female population. Both off-springs are made from these parents and it is described by Eq. (6),

$$\begin{cases} m_{offspring1} = Lm + (1-L)f \\ m_{offspring2} = Lf + (1-L)\,m \end{cases} \quad (6)$$

Now L is a randomly generated number in $[0,1]$, m refers to the male parent, and f indicates the female parent.

The MFO method derives a fitness function to obtain high efficiency of classification. It determines a positive integer to characterize the best outcome of the candidate solution. The decline of classifier error rate is assumed as the fitness function.

$$fitness(x_i) = ClassifierErrorRate(x_i)$$

$$= \frac{No.of\ misclassified\ samples}{Total\ No.of\ samples} * 100 \quad (7)$$

3.4. ELM-based Classification

At the final stage, the ELM model can be used for classification process. ELM is applied for single-hidden layer feedforward neural network (SLFN) where hidden layer (HL) need not be neuron [21]. As long as activation function of the neuron is non-linear piecewise continuous, the hidden node in ELM is generated randomly, unlike other NNs with backpropagation (BP). The weights between the output and the hidden layers have analytical solutions and are evaluated by the following formula. There exist two stages in training of ELM: feature mapping and output weight. ELM feature map: Assume input dataset $x \in \mathbb{R}^D$, the output of ELM for generalized SLFN is

$$f(x) = \sum_{i=1}^{L} \beta_i\, h_i(x) = h(x)\beta, \quad (8)$$

Here the output vector of the HL is $h(x) = [h_1(x), \cdots, h_L(x)]$ and the output weights between the output layer (m nodes) and the hidden layer (L nodes) are $\beta = [\beta_1, \cdots, \beta_L]^T$. The process of getting h is named ELM feature mapping that map input dataset from $\mathbb{R}^D$ to the feature space $\mathbb{R}^L$. In real-time application, h is defined by Eq. (9)

$$h_i(x) = g(a_i, b_i, x), a_i \in \mathbb{R}^D, b_i \in \mathbb{R}, \quad (9)$$

Now activation function satisfying ELM universal approximation ability theorem is $g(a; b, x)$. Indeed, any non-linear piecewise continuous functions are utilized as h activation function. The parameter h is generated at random according to the continuous likelihood distribution. Figure 2 depicts the infrastructure of ELM.

ELM output weight: Assume a training sample set $(x_i, t_i)_{i=1}^n$ with $t_i = [0, \cdots, 0, 1_j, 0, \cdots, 0_m]^T$ the class indicator of x_i, ELM aim is to reduce the training error and the Frobenius norm of output weight:

$$\min_{\beta,\xi} \frac{\omega}{2} \sum_{i=1}^{\uparrow l} \| \xi \|_2^2 + \frac{1}{2} \|\beta\|_F^2,\ s.t.\, \beta h(x_i) = t_i - \xi_i,\ \forall \in 1,2,\ldots,n, \quad (10)$$

In Eq. (10), the training errors of the i^{th} samples are ξ_i, the number of samples is n, and a regularization parameter which trade-offs the norm of output weight and training error is ω. The Frobenius norm is $\|\cdot\|_F^2$.

The optimization problem is effectively resolved. Particularly, according to the Woodbury identity the optimum β is systematically attained as follows:

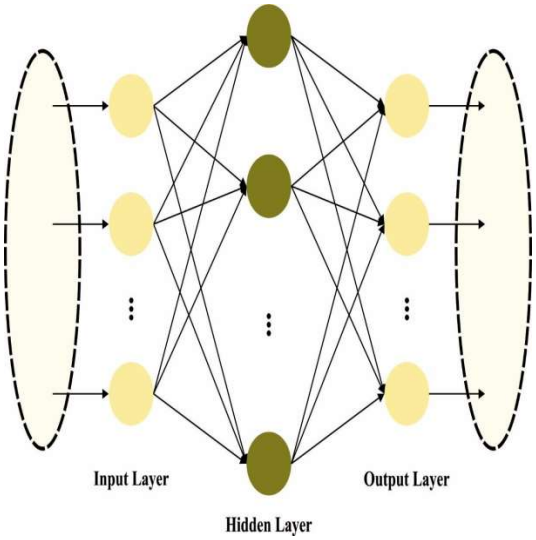

Figure 2: ELM structure

$$\beta^{\star} = \begin{cases} \left(H^T H + \frac{I_L}{\omega}\right)^{-1} H^T T \; if \; L \leq \mathrm{k} \\ H^T \left(HH^T + \frac{I_\mathrm{n}}{\omega}\right)^{-1} T \; otherwise \end{cases} \quad (11)$$

In Eq. (11), I_n and I_L are identity matrices and H is the output matrix of HL (randomized matrix).

$$H = \begin{bmatrix} h(x_1) \\ \vdots \\ h(x_\mathrm{n}) \end{bmatrix} = \begin{bmatrix} h_1(x_1) & \dots & h_L(x_1) \\ \vdots & \ddots & \vdots \\ h_1(x_\mathrm{n}) & \dots & h_L(x_\mathrm{n}) \end{bmatrix} \quad (12)$$

4. PERFORMANCE VALIDATION

In this study, the glaucoma detection results of the MFODL-GDC technique is simulated using DRISHTI-GS1 dataset [22] and ACRIMA dataset [23]. The DRISHTI-GS1 Dataset includes 101 samples whereas the ACRIMA dataset comprises 705 samples as defined in Tables 1 and 2. Figure 3 depicts the sample of glaucoma and normal images. Figure 4 represents the visualization of original images, OD, and CD.

Table 1: Details on DRISHTI-GS1 Dataset

DRISHTI-GS1 Dataset	
Class	No. of Samples
Glaucoma	70
Normal	31
Total Samples	101

Table 2: Details on ACRIMA Dataset

ACRIMA Dataset	
Class	No. of Samples
Glaucoma	396
Normal	309
Total Samples	705

Figure 5 exhibits the classifier analysis of the MFODL-GDC technique with test DRISHTI-GS1 database. Figures. 5a-5b shows the confusion matrices given by the MFODL-GDC system at 70:30 of TR Phase/TS Phase. The outcome denotes that the MFODL-GDC methodology could be suitably recognized and classified with normal and Glaucoma classes. Moreover, Figure 5c represents the PR analysis of the MFODL-GDC system. The simulation value shows that the MFODL-GDC technique gets excellent PR performance with each class. Besides, Figure 5d displayed the ROC analysis of the MFODL-GDC methodology. This outcome illustrated that the MFODL-GDC methodology leads to effectual outcomes with higher ROC values with various classes.

Journal of Theoretical and Applied Information Technology
31st July 2024. Vol.102. No. 14

ISSN: 1992-8645 www.jatit.org E-ISSN: 1817-3195

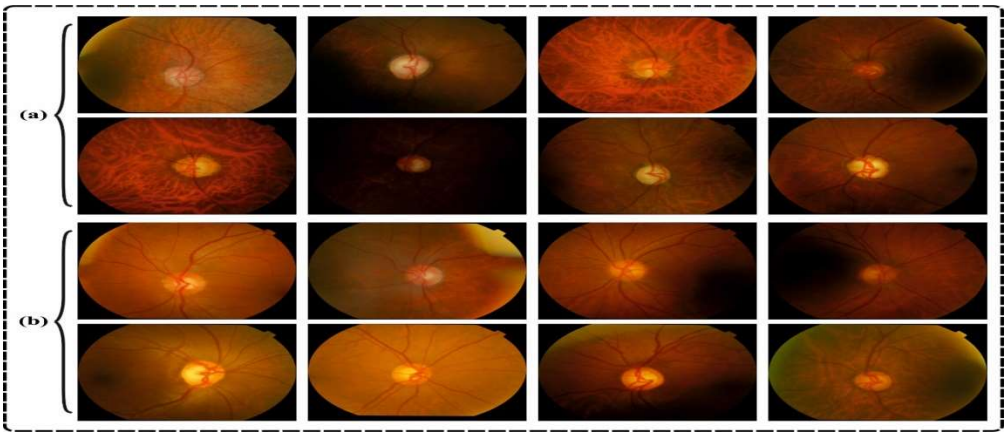

Figure 3: a) Glaucoma Images b) Normal Images

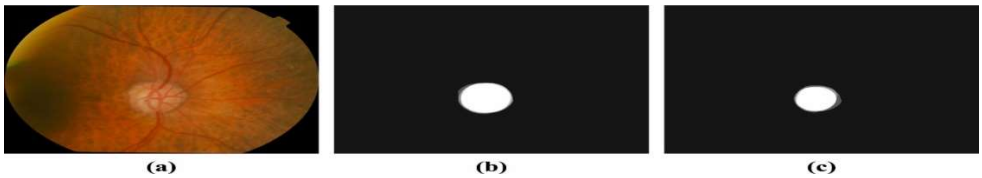

Figure 4: a) Original Image b) Optic Disc c) Cup Disc

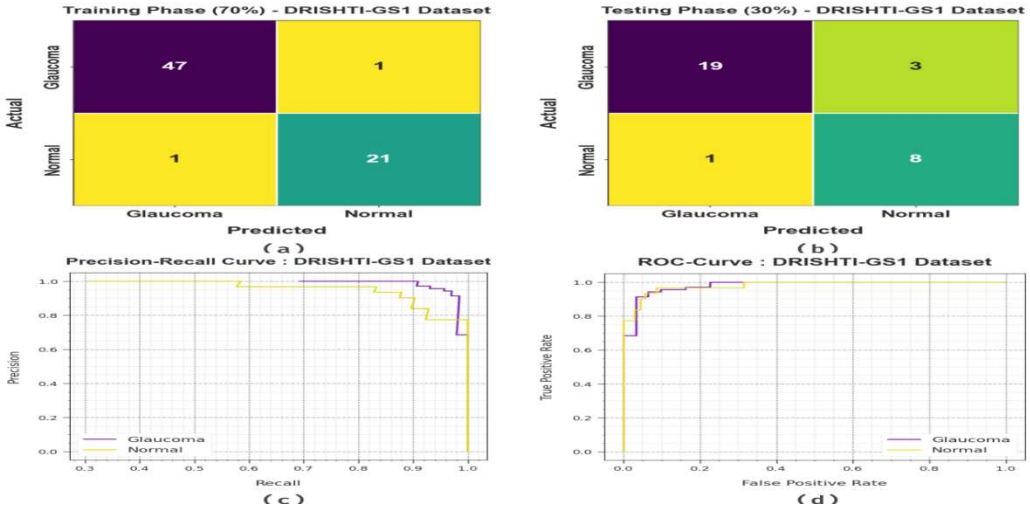

Figure 5: DRISHTI-GS1 dataset (a-b) Confusion Matrix (c-d) PR-curve and ROC-curve

In Table 3, the glaucoma detection results of the MFODL-GDC technique on the DRISHTI-GS1 database is reported. The obtained outcome highlighted that the MFODL-GDC system appropriately recognized the glaucoma and normal samples. With 70% of TR Phase, the MFODL-GDC system attains average $accu_y$ of 97.14%, $prec_n$ of 96.69%, $sens_y$ of 96.69%, $spec_y$ of 96.69%, and F_{score} of 96.69%. Furthermore, with 30% of TS Phase, the MFODL-GDC methodology achieves an average $accu_y$ of 87.10%, $prec_n$ of 83.86%, $sens_y$ of 87.63%, $spec_y$ of 87.63%, and F_{score} of 85.24% respectively.

Table 3: Glaucoma detection analysis of MFODL-GDC approach with DRISHTI-GS1 Dataset

Classes	$Accu_y$	$Prec_n$	$Sens_y$	$Spec_y$	F_{score}

TR Phase (70%)					
Glaucoma	97.14	97.92	97.92	95.45	97.92
Normal	97.14	95.45	95.45	97.92	95.45
Average	97.14	96.69	96.69	96.69	96.69
TS Phase (30%)					
Glaucoma	87.10	95.00	86.36	88.89	90.48
Normal	87.10	72.73	88.89	86.36	80.00
Average	87.10	83.86	87.63	87.63	85.24

Table 4 and Figure 6 illustrate an overall comparative glaucoma detection result of the MFODL-GDC technique on the DRISHTI-GS1 Dataset [24, 25]. The achieved outcome highlighted that the KNN, RF, and SVM algorithms get worse detection rate. Along with that, the DBN and DBN-EHO models have reported slightly increased classification results. However, the MFODL-GDC system demonstrates superior performance with maximum $accu_y$, $sens_y$, and $spec_y$ of 97.14%, 96.69%, and 96.69%, respectively.

Table 4 Comparison analysis of MFODL-GDC approach with other models DRISHTI-GS1 Dataset

DRISHTI-GS1 Dataset			
Classifier	$Accu_y$	$Sens_y$	$Spec_y$
KNN Algorithm	95.34	90.47	93.08
RF Model	94.50	91.34	92.33
SVM Model	95.86	96.07	96.07
DBN Model	96.23	95.56	96.02
DBN–EHO	96.95	95.56	95.44
MFODL-GDC	97.14	96.69	96.69

Figure 7 shows the classifier analysis of the MFODL-GDC system with test ACRIMA database. Figures 7a-7b shows the confusion matrix offered by the MFODL-GDC technique at 70:30 of TR Phase/TS Phase.

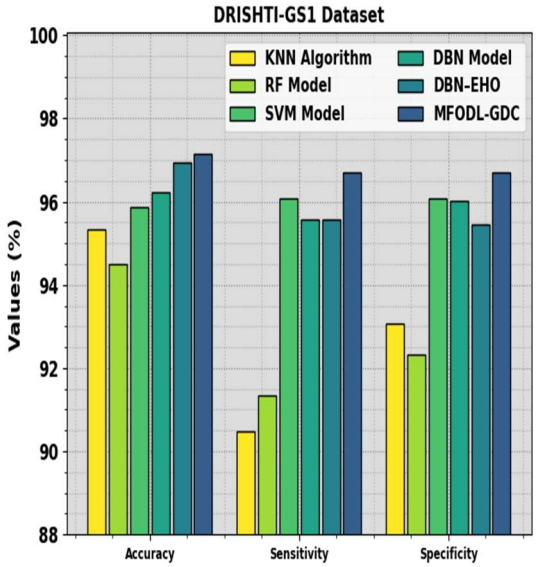

Figure 6: Comparison analysis of the MFODL-GDC approach on the DRISHTI-GS1 database

The outcome exhibits that the MFODL-GDC methodology could be properly recognized and classified with normal and Glaucoma classes. Additionally, Figure 7c exhibits the PR analysis of the MFODL-GDC system. This figure represents that the MFODL-GDC method obtains greater PR performance with each class. Also, Figure 7d presented the ROC analysis of the MFODL-GDC methodology. This outcome represented that the MFODL-GDC algorithm leads to effectual outcomes with higher ROC values with various classes.

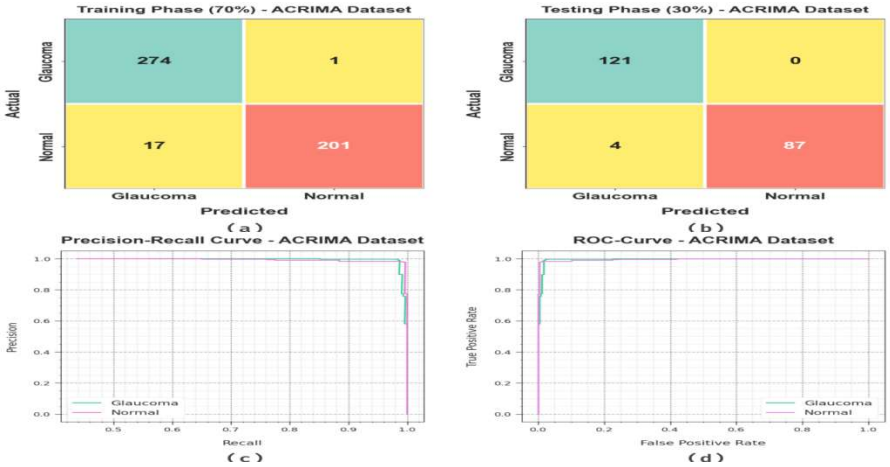

Figure 7: ACRIMA dataset (a-b) Confusion Matrix (c-d) PR-curve and ROC-curve

Table 5: Glaucoma detection analysis of MFODL-GDC approach with ACRIMA Database

Class	$Accu_y$	$Prec_n$	$Sens_y$	$Spec_y$	F_{score}
TR Phase (70%)					
Glaucoma	96.35	94.16	99.64	92.20	96.82
Normal	96.35	99.50	92.20	99.64	95.71
Average	96.35	96.83	95.92	95.92	96.27
TS Phase (30%)					
Glaucoma	98.11	96.80	100.00	95.60	98.37
Normal	98.11	100.00	95.60	100.00	97.75
Average	98.11	98.40	97.80	97.80	98.06

In Table 5, the glaucoma detection analysis of the MFODL-GDC method with the ACRIMA dataset can be computed. The obtained outcome pointed out that the MFODL-GDC system appropriately recognized the glaucoma and normal samples. According to 70% of TR Phase, the MFODL-GDC methodology achieves average $accu_y$ of 96.35%, $prec_n$ of 96.83%, $sens_y$ of 95.92%, $spec_y$ of 95.92%, and F_{score} of 96.27%. Also, based on 30% of TS Phase, the MFODL-GDC system gets average $accu_y$ of 98.11%, $prec_n$ of 98.40%, $sens_y$ of 97.80%, $spec_y$ of 97.80%, and F_{score} of 98.06% respectively.

Table 6 and Figure 8 represents an overall comparison glaucoma detection analysis of the MFODL-GDC algorithm with the ACRIMA database. The attained outcome shows that the KNN, RF, and SVM methodologies gets poorer detection rate. Then, the DBN and DBN-EHO models attains moderately increased classification outcomes. But, the MFODL-GDC system indicates excellent performance with greater $accu_y$, $sens_y$, and $spec_y$ of 97.14%, 96.69%, and 96.69%, correspondingly.

Table 6: Comparison analysis of the MFODL-GDC approach with other models on ACRIMA database

ACRIMA Dataset			
Classifier	$Accu_y$	$Sens_y$	$Spec_y$
SVM Model	97.06	96.64	96.12
DBN Algorithm	97.26	97.16	97.06
DBN–EHO	97.34	97.10	97.20
MFODL-GDC	98.11	97.80	97.80

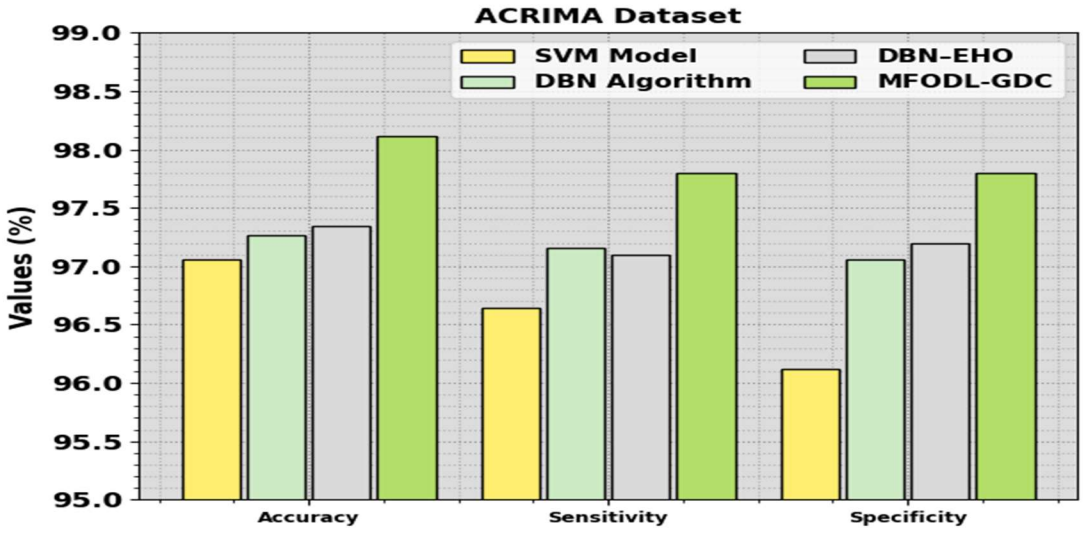

Figure 8: Comparison analysis of the MFODL-GDC approach on ACRIMA database

Thus, the MFODL-GDC technique can be employed for accurate glaucoma detection process.

Various approaches to automated glaucoma detection using retinal fundus images have been explored. Lenka et al. [11] presented a multi-task deep learning model, achieving segmentation and classification tasks with MobileNetv2 and GCN. Kamara et al. [12] utilized feature selection techniques, combining superpixel methods and SVM in a two-stage process. Shyamalee and Meedeniya [13] applied attention U-Net with CNN models for image subdivision and preprocessing. Phasuk et al. [14] proposed an ensemble model for glaucoma screening, employing ANNs for final classification.

In comparison, the MFODL-GDC technique surpasses traditional and advanced models on the DRISHTI-GS1 dataset, as shown in Table 3. It achieved high accuracy, precision, sensitivity, and specificity during both training and testing phases. Notably, during the TR phase, MFODL-GDC attains an average accuracy of 97.14% and during the TS phase, it maintains strong performance with an average accuracy of 87.10%. Additionally, Table 4 and Figure 6 demonstrate the superiority of MFODL-GDC over other models, with maximum accuracy, sensitivity, and specificity of 97.14%, 96.69%, and 96.69%, respectively.

Further validation on diverse datasets and clinical settings is crucial for practical implementation. Overall, while the MFODL-GDC technique represents a significant advancement, addressing challenges related to data quality and interpretability is essential for its broader adoption in clinical practice.

5. CONCLUSION

In this study, we have devised and developed an automated glaucoma detection process, named technique on Retinal Fundus Images. The MFODL-GDC technique aims to segment and classify the retinal fundus images for the identification of Glaucoma. It comprises several stages of operations namely image preprocessing, QCN segmentation, DenseNet feature extraction, MFO-based hyperparameter tuning, and ELM classification. Moreover, the MFODL-GDC technique uses DenseNet121 model for feature extraction and its hyperparameter tuning process can be performed by the use of the MFO algorithm. Finally, the ELM model can be exploited for the detection and classification process. The extensive performance validation of the MFODL-GDC technique is tested on benchmark dataset. The

widespread comparison study stated the supremacy of the MFODL-GDC technique over recent approaches.

Some of the strengths of this work includes innovative approach integrating multiple stages, comprehensive methodology utilizing advanced techniques like DenseNet121 and MFO-based hyperparameter tuning, extensive performance validation on benchmark datasets, and comparative analysis demonstrating superiority over existing methods. This work also embraces few weaknesses including dependency on quality and quantity of datasets, complexity and computational cost, interpretability issues with Deep Learning models, need for thorough evaluation of MFO algorithm's efficacy, and clarification on the diversity of validation datasets. Overall, this research work profoundly overwhelms in predicting retinal fundus images with optimal performance.

REFERENCES:

[1] Borwankar, S.; Sen, R.; Kakani, B. Improved Glaucoma Diagnosis Using Deep Learning. In Proceedings of the 2020 IEEE International Conference on *Electronics, Computing and Communication Technologies (CONECCT)*, Bangalore, India, 2–4 July 2020; pp. 2–5.

[2] Huang, X.; Sun, J.; Gupta, K.; Montesano, G.; Crabb, D.P.; Garway-Heath, D.F.; Brusini, P.; Lanzetta, P.; Oddone, F.; Turpin, A.; et al. Detecting Glaucoma from Multi-Modal Data Using Probabilistic Deep Learning. Front. Med. 2022, 9, 923096.

[3] Mahdi, H.; Abbadi, N. El Glaucoma Diagnosis Based on Retinal Fundus Image: A Review. *Iraqi J. Sci.* 2022, 63, 4022–4046.

[4] Hemelings, R.; Elen, B.; Barbosa-Breda, J.; Blaschko, M.B.; De Boever, P.; Stalmans, I. Deep Learning on Fundus Images Detects Glaucoma beyond the Optic Disc. Sci. Rep. 2021, 11, 20313.

[5] Saeed, A.Q.; Abdullah, S.N.H.S.; Che-Hamzah, J.; Ghani, A.T.A. Accuracy of Using Generative Adversarial Networks for Glaucoma Detection: Systematic Review and Bibliometric Analysis. *J. Med. Internet Res*. 2021, 23, e27414.

[6] Mohamed, N.A.; Zulkifley, M.A.; Zaki, W.M.D.W.; Hussain, A. An Automated Glaucoma Screening System Using Cup-to-Disc Ratio via Simple Linear Iterative Clustering Superpixel Approach. *Biomed. Signal Process. Control*. 2019, 53, 101454.

[7] Natarajan, D.; Sankaralingam, E.; Balraj, K.; Karuppusamy, S. A Deep Learning Framework for Glaucoma Detection Based on Robust Optic Disc Segmentation and Transfer Learning. *Int. J. Imaging Syst. Technol.* 2022, 32, 230–250.

[8] Norouzifard, M.; Nemati, A.; Gholamhosseini, H.; Klette, R.; Nouri-Mahdavi, K.; Yousefi, S. Automated Glaucoma Diagnosis Using Deep and Transfer Learning: Proposal of a System for Clinical Testing. In Proceedings of the 2018 *International Conference on Image and Vision Computing New Zealand (IVCNZ)*, Auckland, New Zealand, 19–21 November 2018.

[9] Xue, Y.; Zhu, J.; Huang, X.; Xu, X.; Li, X.; Zheng, Y.; Zhu, Z.; Jin, K.; Ye, J.; Gong, W.; et al. A Multi-Feature Deep Learning System to Enhance Glaucoma Severity Diagnosis with High Accuracy and Fast Speed. *J. Biomed. Inform.* 2022, 136, 104233.

[10] Raghavendra, U.; Fujita, H.; Bhandary, S.V.; Gudigar, A.; Tan, J.H.; Acharya, U.R. Deep Convolution Neural Network for Accurate Diagnosis of Glaucoma Using Digital Fundus Images. *Inf. Sci.* 2018, 441, 41–49.

[11] Lenka, S., Mayaluri, Z.L., Panda, G. and Nayak, S.R., 2023. Glaucoma Detection from Retinal Fundus Images using Graph Convolution Based Multi-task Model.

[12] Kamara, O.M., Asad, A.H. and Hefny, H.A., 2023, September. Automated Diagnoses Glaucoma Approach in Retinal Fundus Images Using Support Vector Machine. In International Conference on *Advanced Intelligent Systems and Informatics* (pp. 368-379). Cham: Springer Nature Switzerland.

[13] Shyamalee, T. and Meedeniya, D., 2022. Glaucoma detection with retinal fundus images using segmentation and classification. *Machine Intelligence Research,* 19(6), pp.563-580.

[14] Phasuk, S., Poopresert, P., Yaemsuk, A., Suvannachart, P., Itthipanichpong, R., Chansangpetch, S., Manassakorn, A., Tantisevi, V., Rojanapongpun, P. and Tantibundhit, C., 2019, July. Automated

glaucoma screening from retinal fundus image using deep learning. In 2019 41st annual international conference of *the IEEE engineering in medicine and biology society (EMBC)* (pp. 904-907). IEEE.

[15] Sharma, A., Aggarwal, M., Roy, S.D. and Gupta, V., 2019, October. Automatic glaucoma diagnosis in digital fundus images using convolutional neural network. In 2019 5th *International Conference on Signal Processing, Computing and Control (ISPCC)* (pp. 160-165). IEEE.

[16] Manikandan, T., Satheesh Kumar, S., Joshua Kumaresan, S., Shobana Priya, M.S. and Priyanka, R., 2019. Glaucoma Detection in Retinal Images using Automatic Thresholding and Marker-Controlled Watershed Transformation.

[17] Yussof, W.N.J.H.W., Man, M., Umar, R., Zulkeflee, A.N., Awalludin, E.A. and Ahmad, N., 2022. Enhancing Moon Crescent Visibility Using Contrast-Limited Adaptive Histogram Equalization and Bilateral Filtering Techniques. *Journal of Telecommunications and Information Technology*, (1).

[18] Sasikumar, N. and Senthilkumar, M., 2023. *Deep Convolutional Generative* Adversarial Networks for Automated Segmentation and Detection of Lung Adenocarcinoma Using Red Deer Optimization Algorithm. Information Technology and Control, 52(3), pp.680-692.

[19] Hasan, N., Bao, Y., Shawon, A. and Huang, Y., 2021. DenseNet convolutional neural networks application for predicting COVID-19 using CT image. *SN computer science,* 2(5), p.389.

[20] Xu, H., Zhao, M., Xue, F., Zhang, X. and Sun, L., 2023. An Improved Mayfly Algorithm with Shading Detection for MPPT of Photovoltaic Systems. *IEEE* Access.

[21] Wang, Y., Xie, Z., Xu, K., Dou, Y. and Lei, Y., 2016. An efficient and effective convolutional auto-encoder extreme learning machine network for 3d feature learning. *Neurocomputing,* 174, pp.988-998.

[22] https://www.kaggle.com/datasets/lokeshsaipureddi/drishtigs-retina-dataset-for-onh-segmentation

[23] Elangovan, P.; Nath, M.K. Glaucoma Assessment from Color Fundus Images Using Convolutional Neural Network. Int. J. Imaging Syst. Technol. 2021, 31, 955–971.

[24] Zedan, M.J., Zulkifley, M.A., Ibrahim, A.A., Moubark, A.M., Kamari, N.A.M. and Abdani, S.R., 2023. Automated Glaucoma Screening and Diagnosis Based on Retinal Fundus Images Using Deep Learning Approaches: A Comprehensive Review. *Diagnostics,* 13(13), p.2180.

[25] Ali, M.A., Balasubramanian, K., Krishnamoorthy, G.D., Muthusamy, S., Pandiyan, S., Panchal, H., Mann, S., Thangaraj, K., El-Attar, N.E., Abualigah, L. and Abd Elminaam, D.S., 2022. Classification of glaucoma based on elephant-herding optimization algorithm and deep belief network. *Electronics*, 11(11), p.1763.